Acta Crystallographica Section D
Biological Crystallography
ISSN 0907-4449

Structures of two mutants that probe the role in iron release of the dilysine pair in the N-lobe of human transferrin

Heather M. Baker,[a] Didier Nurizzo,[a]‡ Anne B. Mason[b] and Edward N. Baker[a,c]*

[a]School of Biological Sciences, University of Auckland, Private Bag 92019, Auckland, New Zealand, [b]Department of Biochemistry, University of Vermont College of Medicine, Burlington, VT 05405, USA, and [c]Department of Chemistry, University of Auckland, Private Bag 92019, Auckland, New Zealand

‡ Present address: European Synchrotron Radiation Facility, BP-220, Grenoble, France.

Correspondence e-mail: ted.baker@auckland.ac.nz

Received 12 October 2006
Accepted 3 January 2007

PDB References: transferrin N-lobe, K206E mutant, 2o84, r2o84sf; K206E/K296E mutant, 2o7u, r2o7usf.

Iron uptake by humans depends on the ability of the serum protein transferrin (Tf) to bind iron as Fe^{3+} with high affinity but reversibly. Iron release into cells occurs through receptor-mediated endocytosis, aided by the lower endosomal pH of about 5.5. The protonation of a hydrogen-bonded pair of lysines, Lys206 and Lys296, adjacent to the N-lobe iron site of Tf has been proposed to create a repulsive interaction that stimulates domain opening and iron release. The crystal structures of two mutants, K206E (in which Lys206 is mutated to Glu) and K206E/K296E (in which both lysines are mutated to Glu), have been determined. The K206E structure (2.6 Å resolution; $R = 0.213$, $R_{\rm free} = 0.269$) shows that a salt bridge is formed between Glu206 and Lys296, thus explaining the drastically slower iron release by this mutant. The K206E/K296E double-mutant structure (2.8 Å resolution; $R = 0.232$, $R_{\rm free} = 0.259$) shows that the Glu296 side chain moves away from Glu206, easing any repulsive interaction and instead interacting with the iron ligand His249. The evident conformational flexibility is consistent with an alternative model for the operation of the dilysine pair in iron release in which it facilitates concerted proton transfer to the tyrosine ligand Tyr188 as one step in the weakening of iron binding.

1. Introduction

Proteins of the transferrin family play a critical role in iron metabolism in animals through their ability to sequester, solubilize and transport iron as Fe^{3+} (Aisen & Harris, 1989; Baker, 1994). The two principal transferrin family members in higher animals, serum transferrin (Tf) and lactoferrin (Lf), have very similar structures and binding properties, but fulfil specialized roles. Tf binds dietary iron, transports it in serum and delivers it to cells through a process of receptor-mediated endocytosis (Klausner *et al.*, 1983; Aisen, 1998), whereas Lf is found in secretory fluids and white blood cells, where it binds iron primarily to provide protection against the toxic effects of free iron (Brock, 2002).

The three-dimensional structures of Tf (Bailey *et al.*, 1988; Hall *et al.*, 2002), Lf (Anderson *et al.*, 1987, 1989) and the avian egg-white homologue ovotransferrin (oTf; Kurokawa *et al.*, 1995) have been well established by X-ray crystallography. In each case the single polypeptide chain is folded into two globular lobes representing its N-terminal and C-terminal halves; these lobes, referred to as the N- and C-lobes, are homologous, sharing ∼40% sequence identity, very similar structures and a single iron-binding site each. The iron-binding site of each lobe is enclosed between two domains, labelled N1

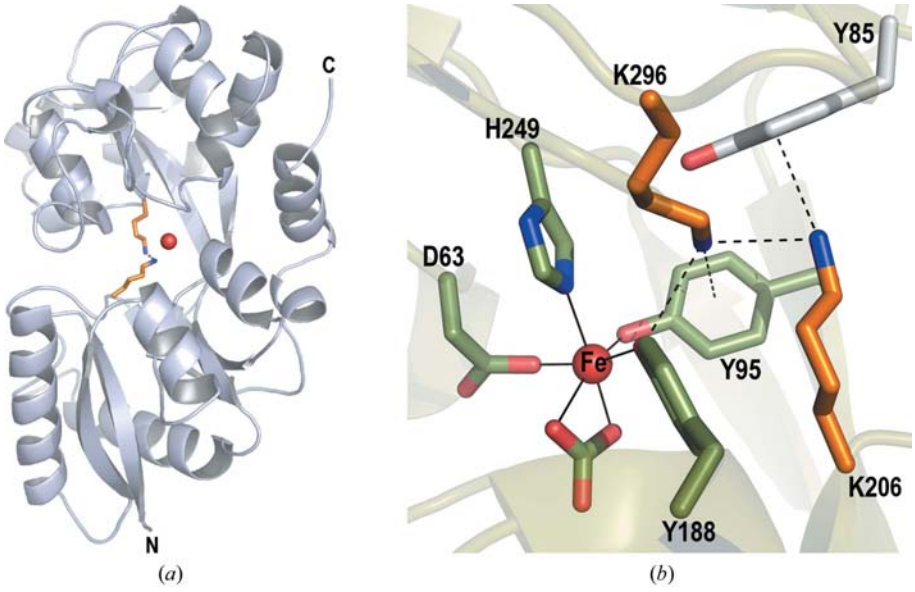

Figure 1
Dilysine interaction in the N-lobe of transferrin. (*a*) Ribbon diagram showing the approach of Lys296 from domain N1 (lower) to Lys206 from domain N2 (upper) adjacent to the bound Fe atom (red sphere). (*b*) Interactions made by the ε-amino group of Lys296: hydrogen bonds (broken lines) to Lys206 N^{ζ}, Tyr188 O^{η} and the aromatic ring of Tyr95. This and the other figures were prepared using *PyMOL* (DeLano, 2002).

and N2 or C1 and C2, which provide four protein ligands (two Tyr, one Asp and one His) together with a synergistically bound carbonate ion (Anderson *et al.*, 1989; Baker, 1994).

A fundamental functional question concerns the mechanism through which iron is bound extremely tightly by Tf, with a dissociation constant K_d of $\sim 10^{-22}$ *M* (Aisen *et al.*, 1978), but is nevertheless able to be efficiently released into cells for utilization (Baker *et al.*, 2004). This is achieved partly by receptor action, which mediates release from the C-lobe (Bali & Aisen, 1991). Iron release from the N-lobe, however, appears to depend on the lower endosomal pH of $\sim$5.5; at this pH bound Fe^{3+} is released spontaneously from the N-lobe of Tf.

The recombinant N-lobe half-molecule of human Tf (Tf_N), comprising residues 1–337, has proved to be an excellent model for investigating the structural basis for iron release because of its tractability for mutational, spectroscopic and crystallographic studies (Woodworth *et al.*, 1991). Structurally, it has been shown that iron release is associated with a large conformational change from the closed structure that is characteristic of the iron-bound form to an open structure in which one of the domains has rotated by $\sim 60^{\circ}$ relative to the other, generating a wide-open binding cleft. Similar conformational changes are seen for the whole molecule and for Tf_N (Jeffrey *et al.*, 1998; Wally *et al.*, 2006). The movement is facilitated by a hinge in two β-strands at the back of the iron-binding site. Several protonation events are postulated to be involved in facilitating this change at low pH, including conversion of the carbonate ligand to bicarbonate (MacGillivray *et al.*, 1998), protonation of the histidine or tyrosine ligands (el Hage Chahine & Pakdaman, 1995; Jeffrey *et al.*, 1998) and protonation of a hydrogen-bonded pair of lysine residues, Lys206 from the N2 domain and Lys296 from the N1 domain (Fig. 1*a*). The latter residues form what has been referred to as a 'dilysine trigger' that stimulates iron release (Dewan *et al.*, 1993).

Disruption of the dilysine interaction by mutation of Lys206 and/or Lys296 drastically slows iron release at pH 5.6 (Steinlein *et al.*, 1998; He *et al.*, 1999, He & Mason, 2002), confirming an important role for these residues. However, the mechanism through which they exert their effect has been a subject of debate. The existence of a hydrogen bond between them (Fig. 1*b*) implies that one is in its unprotonated form, leading to the suggestion that protonation of this dilysine pair would cause repulsion and domain opening, hence the term 'dilysine trigger'. Theoretical studies indicate that Lys206 does indeed have an abnormally low pK_a, but also suggest that protonation of the dilysine pair is not in itself sufficient to promote domain opening (Rinaldo & Field, 2003). Other observations that need to be reconciled include the fact that mutation of both lysines to Glu does not seem to produce an equivalent repulsion between the resulting negative charges, as the K206E/K296E mutant of Tf has much more stable binding than wild-type Tf (He *et al.*, 1999). Likewise, several Lfs have lysines at analogous positions to the dilysine-pair residues in Tf, but no hydrogen-bonded interaction occurs as one of the lysines is oriented differently (Moore *et al.*, 1997; Peterson *et al.*, 2000). Why does Tf not behave similarly, when its structure appears to be extremely similar in this region?

Here, we present crystal structures of two mutants of the N-lobe half-molecule of human Tf, demonstrating that mutation of Lys206 to Glu generates an interdomain ion pair that drastically stabilizes iron binding, but that when both Lys206 and Lys296 are simultaneously mutated to Glu the side chain of Glu296 is re-oriented in order to keep the negative charges apart. This observation, when coupled with other structural, mutational and theoretical data, leads to a re-evaluation of the role of the dilysine pair in iron release.

2. Materials and methods

2.1. Protein production

The K206E and K206E/K296E mutants were prepared by PCR-based mutagenesis of a construct encoding the N-terminal half-molecule of human transferrin, Tf_N, comprising residues 1–337 of the native protein. DNA sequencing confirmed the correctness of each mutant construct. The recombinant proteins were then expressed from baby hamster

Table 1
Data-collection statistics.

Values in parentheses are for the outermost resolution shell.

	K206E	K206E/K296E
Space group	$P2_12_12_1$	$C2$
Unit-cell parameters (Å, °)	a = 44.2, b = 57.3, c = 135.6	a = 169.5, b = 97.9, c = 209.0, β = 90.01
Resolution range (Å)	22.7–2.60 (2.74–2.60)	48.0–2.80 (2.95–2.80)
Measured reflections	35487 (5081)	273627 (39423)
Unique reflections	10917 (1576)	83306 (12120)
$R_{\rm merge}$	0.139 (0.377)	0.074 (0.406)
Multiplicity	3.3 (3.2)	3.3 (3.3)
Completeness	98.5 (100.0)	98.5 (98.8)
Mean $I/\sigma(I)$	9.0 (3.0)	16.4 (3.2)

kidney (BHK) cells containing the relevant cDNA in the pNUT vector and were purified from the culture medium as described previously (Woodworth *et al.*, 1991; He *et al.*, 1999). Using this protocol, the proteins are obtained in predominantly iron-saturated form. To ensure full iron saturation, however, and the incorporation of bicarbonate as the synergistic anion, a slight excess of ferric nitrilotriacetate (FeNTA) was added to a buffer solution at pH 7.4 containing the protein and 0.1 *M* sodium bicarbonate.

2.2. Protein crystallization

Immediately before crystallization trials were carried out, the protein was passed down a gel-filtration column (Superdex 75 HR 10/30) equilibrated in 0.1 *M* ammonium bicarbonate pH 7.4. Fractions were tested for monodispersity by dynamic light scattering (Protein Solutions DynaPro-MS200). The ratio $C_{\rm p}/R_{\rm h}$, where $C_{\rm p}$ is a measure of the size distribution, or polydispersity, and $R_{\rm h}$ is the mean hydrodynamic radius, was used as an index and only those samples with a $C_{\rm p}/R_{\rm h}$ ratio of less than 14 were used. Both mutants were crystallized at 291 K under the same conditions using the hanging-drop method, in which equal volumes of protein solution (35 mg ml^{-1} protein in 0.1 *M* ammonium bicarbonate pH 7.4) and reservoir solution were mixed. Crystals were obtained by microseeding with wild-type $\rm FeTf_N$ crystals, as performed successfully for other transferrin mutants (Nurizzo *et al.*, 2001; Baker *et al.*, 2001). Crystals grew from a 50:50 mixture of mutant protein solution and reservoir solution (0.2 *M* potassium acetate pH 7.4 containing 16–22% PEG 3350), with crystals of each mutant appearing in a few days. The K206E crystals were isomorphous with the form 1 wild-type $\rm FeTf_N$ crystals, with one molecule in the asymmetric unit, space group $P2_12_12_1$ and unit-cell parameters a = 44.2, b = 57.3, c = 135.6 Å. The K206E/K296E double-mutant crystals, however, appeared under the same conditions but in a different crystal form, space group $C2$, with unit-cell parameters a = 169.5, b = 97.9, c = 209.0 Å, β = 90.01°. This was consistent with the presence of 6–12 molecules in the asymmetric unit, assuming a solvent content in the range 40–70%.

2.3. Data collection and processing

X-ray diffraction data were collected at 110 K from crystals that had been flash-frozen after soaking in a cryoprotectant comprising 0.2 *M* potassium acetate pH 7.4 with 35% PEG 3350. Data were collected using Cu $K\alpha$ radiation (λ = 1.5418 Å) from a Rigaku RU-300 rotating-anode generator equipped with Osmic mirrors and a MAR345 imaging-plate detector. Both data sets were integrated with *MOSFLM* and scaled and merged with *SCALA* from the *CCP*4 suite (Collaborative Computational Project Number 4, 1994). Data sets were more than 98% complete to maximum resolutions of 2.6 and 2.8 Å, respectively, for the K206E and K206E/K296E mutants. Full data statistics are given in Table 1.

2.4. Structure determination and refinement

The K206E crystals were isomorphous with form 1 wild-type $\rm FeTf_N$ crystals and the 1.6 Å structure of the latter (PDB code 1a8e; MacGillivray *et al.*, 1998) was therefore used as an initial model after removal of the Fe^{3+} and CO_3^{2-} ions, all solvent molecules and the side chain of residue 206. The structure was refined with *CNS* (Brünger *et al.*, 1998). Cycles of rigid-body refinement, first as the whole molecule and then as the two domains, were followed by simulated annealing between 10 000 and 100 K. Subsequent cycles of refinement were interspersed with manual model building using *Coot* (Emsley & Cowtan, 2004) into *SIGMAA*-weighted $2mF_{\rm o} - DF_{\rm c}$ and $mF_{\rm o} - DF_{\rm c}$ difference electron-density maps. The positions of the Fe^{3+} and CO_3^{2-} ions and the side chain of the mutated residue Glu206 were clearly apparent. Solvent molecules were added automatically in *CNS* but were visually checked in difference maps and only those with good spherical density, reasonable B factors and hydrogen-bond partners with appropriate geometry were retained. All were treated as water molecules, except for one potassium ion that is also present in other $\rm FeTf_N$ structures (Nurizzo *et al.*, 2001; Baker *et al.*, 2001). The final values of R and $R_{\rm free}$ were 21.3 and 26.9%, with approximately 5% of the reflections, randomly chosen, used in the free R calculation.

The K206E/K296E double-mutant structure was solved by molecular replacement using *Phaser* (Storoni *et al.*, 2004), with the 1.6 Å form 1 wild-type $\rm FeTf_N$ structure (PDB code 1a8e) taken as a search model after removal of the Fe^{3+} and CO_3^{2-} ions, all solvent molecules and the side chains of residues 206 and 296. Nine molecules were found with reasonable crystal-packing interactions. After a round of rigid-body refinement, refinement of the structure was continued with *REFMAC* (Murshudov *et al.*, 1997). In each round of refinement, cycles of TLS refinement (with nine TLS groups, one per molecule) were followed by cycles of conventional refinement with isotropic B factors and manual rebuilding with *Coot* (Emsley & Cowtan, 2004). Strict NCS constraints were maintained throughout the refinement. The positions of the Fe^{3+} and CO_3^{2-} ions and the side chains of the two mutated residues Glu206 and Glu296 were clearly apparent in the first electron-density maps. Water molecules were added automatically using the *Find Waters* routine in *Coot* and were checked manually. Only those waters with good spherical density and reasonable B factors and hydrogen-bond geometry and that were present in all nine molecules were retained. The final

Table 2
Refinement and model details.

	K206E	K206E/K296E
Resolution limits (Å)	21.0–2.60	30.0–2.80
Total No. of reflections	10358	78012
Reflections used for R_{free}	521	4132
R factor	0.213	0.232
R_{free}	0.269	0.259
Model details		
Protein atoms	2551	22959 (9 mols)
Water molecules	130	81
Other molecules/ions	1 Fe^{3+}, 1 CO_3^{2-}, 1 K^+	9 Fe^{3+}, 9 CO_3^{2-}
R.m.s. deviations from standard geometry		
Bond lengths (Å)	0.010	0.011
Bond angles (°)	1.3	1.5
Average B factors (Å^2)		
Protein atoms	14.3	58.8
Water molecules	15.4	31.8
Residues in most favoured region of Ramachandran plot (%)	93.8	91.0
PDB code	2o84	2o7u

values of R and R_{free} were 23.2 and 25.9%, with approximately 5% of the reflections, randomly chosen, used in the free R calculation. Full refinement and model statistics are given in Table 2.

2.5. Model completeness and quality

The final model for K206E comprised residues 3–331, one K^+ ion and 129 water molecules, with no electron density being apparent for the N-terminal residues prior to Asp3 or for the C-terminal residues following Cys331. The final model for the double mutant K206E/K296E has nine molecules in the asymmetric unit, with each molecule comprising residues 3–331, and again no electron density observed for residues 1–2. In both structures the protein molecules conform well to standard geometry. Bond lengths and angles are restrained close to the standard values of Engh & Huber (1991) (Table 2) and main-chain torsion angles conform with allowed regions of the Ramachandran plot; for K206E 93.8% of residues are in the most favoured regions, as defined by *MOLPROBITY* (Lovell *et al.*, 2003), and for the K206E/K296E double mutant the figure is 91.0%.

3. Results and discussion

For both mutants, the crystal structures represent the iron-bound form. Structural superpositions onto the parent structure, the wild-type N-terminal half-molecule of human transferrin, Tf_N (MacGillivray *et al.*, 1998), show that in neither case is there any significant change in the overall protein structure or in the closure of the two domains over the bound Fe^{3+} and CO_3^{2-} ions. For the K206E mutant, superposition of the whole molecule onto wild-type Tf_N gives a root-mean-square (r.m.s.) difference in atomic positions of 0.36 Å for 302 C^α atoms, compared with 0.30 and 0.33 Å for the individual domains N1 and N2, respectively; there is a difference of only 1.3° in the relative orientations of the two domains in the wild-type and K206E proteins. Likewise, for the K206E/K296E double mutant the r.m.s. differences when compared with wild-type Tf_N are 0.47, 0.36 and 0.42 Å for the whole molecule and for the N1 and N2 domains, respectively, and the difference in domain orientations corresponds to a rotation of only 1.5°. Similar variations are found for other mutants and for the two crystal forms of wild-type Tf_N and do not seem to have any functional significance. With one intriguing exception, the structure of the iron-binding site also appears to be unchanged in each mutant with respect to bond distances and angles, at least within the resolution limits of the analyses. The one exception is that the Fe—N(His249) bond is distinctly longer in the K206E mutant (2.6 Å) than in wild-type Tf_N (2.1 Å). We do not have a good explanation for this difference, but note that theoretical calculations by Rinaldo & Field (2004) suggest that the bond length in wild-type Tf_N is more consistent with coordinated imidazolate rather than imidazole. This could suggest that the His ligand in K206E is in the imidazole form, with a longer Fe—N bond, perhaps as a result of electrostatic differences that stem from the Lys206Glu mutation.

Importantly, there are specific differences at the mutation sites which bear on the properties of iron binding and release for these mutants and contribute to a better understanding of the mechanisms of iron release by Tf. These differences are detailed below.

3.1. K206E mutant

The mutation of Lys206 to Glu fundamentally alters the interactions between the two domains. In wild-type Tf_N, as in the N-lobes of full-length Tf and oTf, the side-chain amino group of Lys206 is hydrogen bonded (3.0 Å) to that of Lys296 from the other domain. This is possible because the pK_a of Lys206 is abnormal (Rinaldo & Field, 2003) and the amino group is unprotonated and thus able to act as a hydrogen-bond acceptor at the pH of crystallization (pH 7.4). At lower pH, protonation of Lys206 is presumed to abolish the interaction and this 'dilysine trigger' is thus believed to stimulate domain opening and iron release (Dewan *et al.*, 1993; Steinlein *et al.*, 1998; He *et al.*, 1999; Nurizzo *et al.*, 2001). The substitution of Glu in the K206E mutant results in the formation of what appears to be a strong salt bridge (2.6 Å) between Glu206 $O^{\varepsilon 2}$ and Lys296 N^ζ. The new Glu side chain follows the conformation of Lys206 in the parent molecule and the amino group of Lys296 moves about 1 Å to form the salt bridge (Fig. 2). Additional interactions made by the carboxyl group of Glu206 include hydrogen bonds with Ser208 O^γ, Ser298 O^γ and a water molecule, replacing the interactions of Lys206 N^ζ with Ser298 O^γ and a water molecule in wild-type Tf_N. Apart from its salt bridge with Glu206, the environment of Lys296, the other half of the dilysine trigger, hardly changes in the K206E mutant. Lys296 N^ζ still hydrogen bonds (3.1 Å) to the phenolate O atom of the iron ligand Tyr188 and forms an amino–π interaction with the aromatic ring of the other Tyr ligand, Tyr95; the distance of N^ζ from the centre of the ring is unchanged at 3.2 Å.

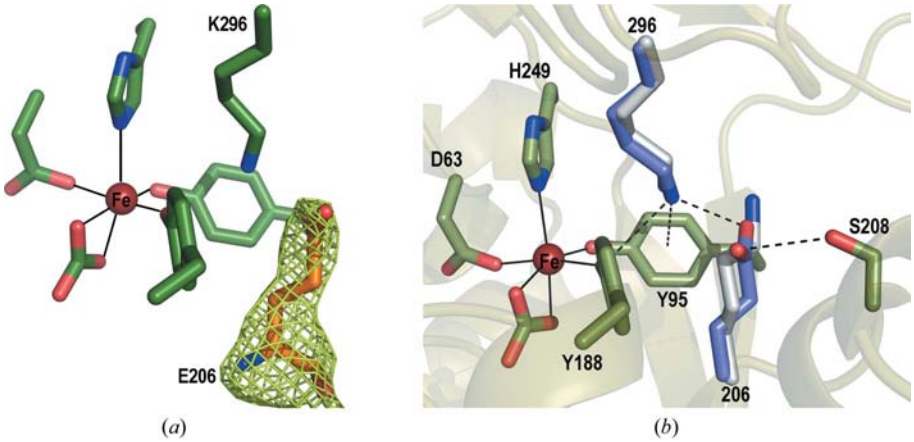

Figure 2
Mutation site in the K206E mutant. (*a*) Bias-removed OMIT density ($F_o - F_c$, contoured at 3σ) for the mutated residue. (*b*) Side chains of Glu206 and Lys296 in the K206E structure, shown in blue, superimposed on Lys206 and Lys296 in the wild-type structure, shown in silver. Other residues common to both proteins are shown in green with atoms coloured by type. Hydrogen bonds are shown as broken lines and covalent metal–ligand bonds are shown as solid black lines.

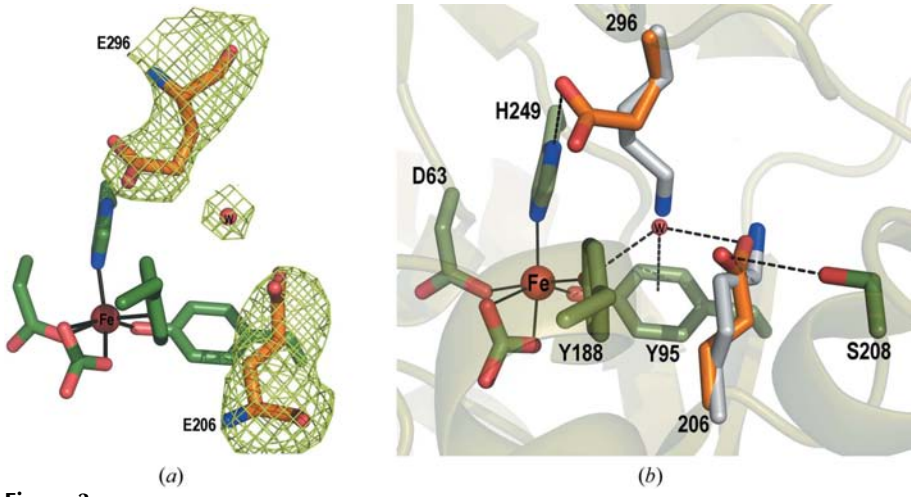

Figure 3
Mutation site in the K206E/K296E double mutant. (*a*) Bias-removed OMIT density ($F_o - F_c$, contoured at 3σ) for the mutated residues. (*b*) Side chains of Glu206 and Glu296 in the mutant structure, shown in gold, superimposed on Lys206 and Lys296 in the wild-type structure, shown in silver. Other residues common to both proteins are shown in green with atoms coloured by type. Hydrogen bonds are shown as broken lines and covalent metal–ligand bonds as solid black lines.

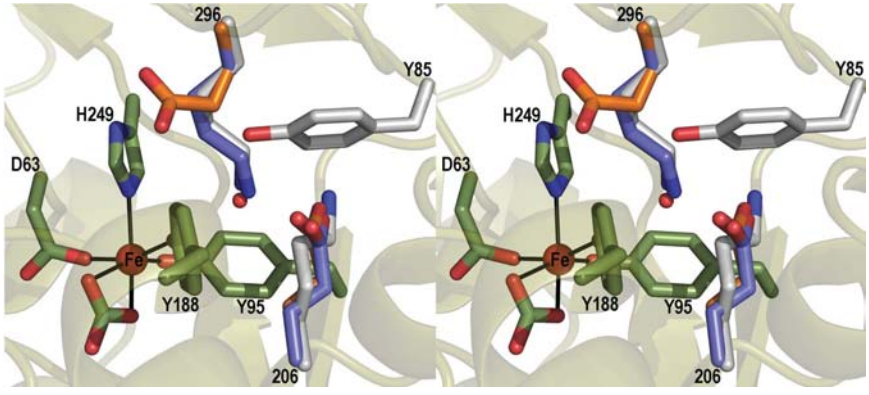

Figure 4
Stereo diagram showing the variation in the positions of residues 206 and 296 in the wild-type N-lobe of Tf (Lys206 and Lys296, in silver), the K206E mutant (Glu206 and Lys296, in blue) and the K206E/K296E double mutant (Glu206 and Glu296, in gold). Residue 206 has the same conformation in each structure. When Glu296 moves away from Glu206 in the double mutant, a water molecule (small red sphere) occupies the site filled by Lys296 N^{ζ} in wild-type Tf.

The overall effect of the K206E mutation is to remove the pH-sensitive dilysine interaction and introduce a new strongly stabilizing interaction in the form of the Glu206–Lys296 salt bridge, while maintaining all other stabilizing interactions. Accordingly, release of iron is slowed drastically for this mutant, reflecting the enhanced stability of the domain-closed structure. The rate constant for iron release to the chelator Tiron is 6.4×10^{-5} min^{-1} at pH 7.4, which is some three orders of magnitude slower than for the wild type (2.25×10^{-2} min^{-1}) and for release to EDTA at pH 5.6, the more physiologically relevant pH, the difference is even greater (1.6×10^{-4} min^{-1} for K206E compared with 4.99 min^{-1} for the wild type; He *et al.*, 1999).

3.2. K206E/K296E mutant

Although structural changes are unsurprisingly more extensive in the double mutant than in K206E, they are still confined to the two mutated residues and their effects are local. As in the K206E mutant, the Glu206 side-chain conformation essentially follows that of the replaced Lys206 side chain, with its carboxyl group displaced about 0.6 Å from the position of the amino group of Lys206 in Tf_N. In this position it makes hydrogen bonds with Ser208 O^{γ}, Ser298 O^{γ} and two water molecules. In contrast, the side chain of Glu296 only follows that of Lys296 as far as its C^{γ} atom; after that, rotation about the C^{β}—C^{γ} bond causes the side chain to bend away to a position where it forms a salt bridge (3.2 Å) through its $O^{\varepsilon 1}$ atom with the iron ligand His249 $N^{\delta 1}$ (Fig. 3). At the same time, its $O^{\varepsilon 2}$ atom is 4.0 Å away from $N^{\eta 2}$ of Arg124, representing another ion-pair interaction (albeit weak). This represents a stable position for the Glu296 side chain (the rotamer is the fourth most common for Glu side chains) and removes it from a potential clash with Glu206; the two carboxyl groups are 6.3 Å apart. One other change that is important for the stability of the K206E/K296E mutant is the presence of a water molecule, W45, at the position occupied by the Lys296 amino group in Tf_N. This water molecule

is hydrogen bonded (2.8 Å) to Glu206 $O^{\varepsilon 2}$ and additionally makes essentially the same interactions that the Lys296 amino group does in Tf_N: hydrogen bonds with Tyr188 O^{η} (2.8 Å), Tyr85 O^{η} (3.0 Å) and an interaction with the π-system of the Tyr95 aromatic ring (3.3 Å).

The principal difference in the K206E/K296E double mutant compared with the wild type is that it has lost the pH-sensitive dilysine interaction. Consistent with this, it displays slower iron-release kinetics than the wild type; $k = 8.99 \times 10^{-2}$ min^{-1} at pH 5.6 compared with 4.99 min^{-1} for the wild type (He *et al.*, 1999). The effect is much less than for the K206E mutant, however, where the new interdomain salt bridge gives a 30 000-fold stabilization. Another informative comparison is with mutants in which Lys206 and Lys296 are mutated to Ala (Nurizzo *et al.*, 2001). Release from the K206E/K296E mutant is only 3.5-fold faster than for the K206A/K296A mutant: 8.99×10^{2} min^{-1} for K206E/K296E compared with 2.48×10^{-2} min^{-1} for K206A/K296A (He *et al.*, 2000). The introduction of the two negative charges on Glu206 and Glu296 thus has a minimal effect *per se* on the destabilization of iron binding. This is explained by the structural flexibility, which allows Glu296 to find an alternative orientation remote from Glu206 while water molecules maintain some of the key interactions in the region it vacates.

3.3. Implications for the role of the dilysine pair in transferrins

A considerable body of structural, mutational, kinetic and theoretical data now allows us to re-evaluate the role of the dilysine pair in transferrins. Theoretical pK_a calculations indicate that it is Lys206 that has an unusually low pK_a, with an estimated value of 7.4 for the closed iron-bound form of the protein, compared with 13.6 for Lys296 (Rinaldo & Field, 2003). Indirect support for the assignment of Lys206 as the nonprotonated lysine comes from structural and mutational studies on human lactoferrin; only when Arg210 (equivalent to Lys206 in Tf) is replaced by nonpositive residues does Lys301 in Lf assume the same position as Lys296 in Tf (Peterson *et al.*, 2000, 2002). From our structural studies, it is also apparent that the conformation of the residue at position 206 is highly constrained. Thus, the Glu206 side chain in the K206E and K206E/K296E mutants of Tf follows the same conformation as Lys206 (Fig. 4), as do the Arg210, Lys210, Glu210, Gln210 and Leu210 side chains in native and mutant Lfs (Peterson *et al.*, 2000, 2002).

In contrast, it is also apparent that the residue at position 296 has considerable flexibility in the conformational space available to it. This is seen in the K206E/K296E and H249E mutants of Tf. In the former Glu296 moves away from Glu206 to form a salt bridge with His249 (Fig. 4) and in the H249E mutant the Lys296 side chain similarly moves away from Lys206, breaking the dilysine-pair interaction, in order to form a salt bridge with the new Glu249 (MacGillivray *et al.*, 2000). Similarly, in the Lf structures two alternative positions have been seen for Lys301, the analogue of Lys296 in Tf. In all native Lf structures, the Lys301 side chain has a quite different orientation to that of Lys296 in Tf, which places its ε-amino group about 6 Å away from the Lys206 ε-amino position. As noted above, however, it can also assume the same conformation as Lys296, provided that a nonpositive residue is present in the Lys206 position (Peterson *et al.*, 2002). These observations suggest that any repulsion between positive charges following protonation of the dilysine pair could be alleviated by movement of Lys296, just as any repulsion between the negative charges of Glu206 and Glu296 is alleviated by the movement of Glu296 in the K206E/K296E mutant structure.

Theoretical simulations of the dynamics of transferrin structures have also indicated that the dilysine-pair residues have sufficient freedom to change conformation without triggering domain opening (Rinaldo & Field, 2003). The conclusion, supported by our structural studies, is that it is unlikely that protonation of the dilysine pair can 'trigger' domain opening simply through the introduction of two opposing positive charges. What, then, is the role of the dilysine pair in iron release from transferrin? Kinetic studies of Tf mutants show clearly that the Lys206–Lys296 interaction has a significant impact on iron release, since the rate of iron release at pH 5.6 is slowed by three orders of magnitude when either residue is mutated to Ala. The pH-stability of iron binding is also significantly enhanced by disruption of the dilysine pair.

We concur with the suggestion of Rinaldo & Field (2003) that the key to understanding the role of the dilysine pair in iron release may lie in the conserved interaction with the iron ligands Tyr95 and Tyr188. A feature of all Tf structures is that the ε-amino group of Lys296 (or its equivalent) occupies a position adjacent to the two tyrosines, hydrogen bonded to the phenolate O atom of Tyr188 and interacting with the π-system of Tyr95 (Dewan *et al.*, 1993; MacGillivray *et al.*, 1998; Nurizzo *et al.*, 2001; Hall *et al.*, 2002). Protonation of the dilysine pair could then result in a concerted proton transfer from Lys206 *via* Lys296 to the phenolate oxygen of Tyr188, with resultant destabilization of iron binding (Rinaldo & Field, 2003). The effects of nonsynergistic anion binding on iron release may also be mediated through the Lys296–Tyr188 interaction, as proposed by He *et al.* (1999). In those structures where a lysine does not fill this position (in Lf and in some mutants of Tf), a water molecule or some other residue (for example, Arg210 in human Lf) occupies the same site and makes the same interactions; proton transfer is still possible but is much less favorable without the dilysine pair as a conduit.

4. Conclusions

The closed structure of the iron-bound form of Tf is maintained primarily by the strength of the bonds between the Fe^{3+} ion and its ligands, which are drawn from the two domains. The present results, taken together with other structural and theoretical studies, support an alternative view of the operation of the 'dilysine trigger' in facilitating iron release from the N-lobe of transferrin. Rather than a repulsive interaction between the two positive charges of the 'dilysine trigger'

causing domain opening, we favour a model in which protonation of the dilysine pair results in concerted proton transfer to the tyrosine ligand Tyr188, as suggested by Rinaldo & Field (2003). Iron release can then be seen as resulting from progressive weakening of the iron coordination through a series of protonation events. These include conversion of the bidentate carbonate ligand to monodentate bicarbonate, protonation and dissociation of the histidine ligand His249 and protonation of Tyr188 *via* the dilysine pair.

This work was supported by the Marsden Fund of New Zealand, the Health Research Council of New Zealand and USPHS grant R01-DK-21739 from the National Institute of Diabetes and Digestive and Kidney Diseases (to ABM). We thank Bryan Anderson, Richard Bunker and Tom Caradoc-Davies for helpful crystallographic discussions.

References

Aisen, P. (1998). *Metal Ions Biol. Syst.* **35**, 585–631.
Aisen, P. & Harris, D. C. (1989). *Physical Biochemistry of the Transferrins*, Vol. 5, *Iron Carriers and Iron Proteins*, edited by T. Loehr, pp. 241–351. New York: VCH Publishers.
Aisen, P., Liebman, A. & Zweier, J. (1978). *J. Biol. Chem.* **253**, 1930–1937.
Anderson, B. F., Baker, H. M., Dodson, E. J., Norris, G. E., Rumball, S. V., Waters, J. M. & Baker, E. N. (1987). *Proc. Natl Acad. Sci. USA*, **84**, 1769–1773.
Anderson, B. F., Baker, H. M., Norris, G. E., Rice, D. W. & Baker, E. N. (1989). *J. Mol. Biol.* **209**, 711–734.
Bailey, S., Evans, R. W., Garratt, R. C., Gorinsky, B., Hasnain, S., Horsburgh, C., Jhoti, H., Lindley, P. F., Mydin, A., Sarra, R. & Watson, J. L. (1988). *Biochemistry*, **27**, 5804–5812.
Baker, E. N. (1994). *Adv. Inorg. Chem.* **41**, 389–463.
Baker, H. M., Anderson, B. F. & Baker, E. N. (2004). *Proc. Natl Acad. Sci. USA*, **100**, 3579–3583.
Baker, H. M., Mason, A. B., He, Q.-Y. & Baker, E. N. (2001). *Biochemistry*, **40**, 11670–11675.
Bali, P. K. & Aisen, P. (1991). *Biochemistry*, **30**, 9947–9952.
Brock, J. H. (2002). *Biochem. Cell Biol.* **80**, 1–6.
Brünger, A. T., Adams, P. D., Clore, G. M., DeLano, W. L., Gros, P., Grosse-Kunstleve, R. W., Jiang, J.-S., Kuszewski, J., Nilges, M., Pannu, N. S., Read, R. J., Rice, L. M., Simonson, T. & Warren, G. L. (1998). *Acta Cryst.* D**54**, 905–921.
Collaborative Computational Project, Number 4 (1994). *Acta Cryst.* D**50**, 760–763.
DeLano, W. L. (2002). *The PyMOL Molecular Graphics System.* http://www.pymol.org/.
Dewan, J. C., Mikami, B., Hirose, M. & Sacchettini, J. C. (1993). *Biochemistry*, **32**, 11963–11968.
el Hage Chahine, J. M. & Pakdaman, R. (1995). *Eur. J. Biochem.* **230**, 1102–1110.
Emsley, P. & Cowtan, K. (2004). *Acta Cryst.* D**60**, 2126–2132.
Engh, R. A. & Huber, R. (1991). *Acta Cryst.* A**47**, 392–400.
Hall, D. R., Hadden, J. M., Leonard, G. A., Bailey, S., Neu, M., Winn, M. & Lindley, P. F. (2002). *Acta Cryst.* D**58**, 70–80.
He, Q.-Y. & Mason, A. B. (2002). *Molecular and Cellular Iron Transport*, edited by D. M. Templeton, pp. 95–123. New York: Marcel Dekker.
He, Q.-Y., Mason, A. B., Nguyen, V., MacGillivray, R. T. A. & Woodworth, R. C. (2000). *Biochem. J.* **350**, 909–915.
He, Q.-Y., Mason, A. B., Tam, B. M., MacGillivray, R. T. A. & Woodworth, R. C. (1999). *Biochemistry*, **38**, 9704–9711.
Jeffrey, P. D., Bewley, M. C., MacGillivray, R. T. A., Mason, A. B., Woodworth, R. C. & Baker, E. N. (1998). *Biochemistry*, **37**, 13978–13986.
Klausner, R. D., Ashwell, J. V., Van Renswoude, J. B., Harford, J. & Bridges, K. (1983). *Proc. Natl Acad. Sci. USA*, **80**, 2263–2267.
Kurokawa, H., Mikami, B. & Hirose, M. (1995). *J. Mol. Biol.* **254**, 196–207.
Lovell, S. C., Davis, I. W., Arendall, W. B. III, De Bakker, P. I. W., Word, J. M., Prisant, M. G., Richardson, J. S. & Richardson, D. C. (2003). *Proteins*, **50**, 437–450.
MacGillivray, R. T. A., Bewley, M. C., Smith, C. A., He, Q.-Y., Mason, A. B., Woodworth, R. C. & Baker, E. N. (2000). *Biochemistry*, **39**, 1211–1216.
MacGillivray, R. T. A., Moore, S. A., Chen, J., Anderson, B. F., Baker, H., Luo, Y., Bewley, M., Smith, C. A., Murphy, M. E., Wang, Y., Mason, A. B., Woodworth, R. C., Brayer, G. & Baker, E. (1998). *Biochemistry*, **37**, 7919–7928.
Moore, S. A., Anderson, B. F., Groom, G. R., Haridas, M. & Baker, E. N. (1997). *J. Mol. Biol.* **274**, 222–236.
Murshudov, G. N., Vagin, A. A. & Dodson, E. J. (1997). *Acta Cryst.* D**53**, 240–255.
Nurizzo, D., Baker, H. M., He, Q.-Y., MacGillivray, R. T. A., Mason, A. B., Woodworth, R. C. & Baker, E. N. (2001). *Biochemistry*, **40**, 1616–1623.
Peterson, N. A., Anderson, B. F., Jameson, G. B., Tweedie, J. W. & Baker, E. N. (2000). *Biochemistry*, **39**, 6625–6633.
Peterson, N. A., Arcus, V. L., Anderson, B. F., Tweedie, J. W., Jameson, G. B. & Baker, E. N. (2002). *Biochemistry*, **41**, 14167–14175.
Rinaldo, D. & Field, M. J. (2003). *Biophys. J.* **85**, 3485–3501.
Rinaldo, D. & Field, M. J. (2004). *Aust. J. Chem.* **57**, 1219–1222.
Steinlein, L. M., Ligman, C. M., Kessler, S. & Ikeda, R. A. (1998). *Biochemistry*, **37**, 13696–13703.
Storoni, L. C., McCoy, A. J. & Read, R. J. (2004). *Acta Cryst.* D**60**, 432–438.
Wally, J., Halbrooks, P. J., Vonrhein, C., Rould, M. A., Everse, S. J., Mason, A. B. & Buchanan, S. K. (2006). *J. Biol. Chem.* **281**, 24934–24944.
Woodworth, R. C., Mason, A. B., Funk, W. D. & MacGillivray, R. T. A. (1991). *Biochemistry*, **30**, 10824–10829.